Pergamon

Geochimica et Cosmochimica Acta, Vol. 66, No. 23, pp. 4119–4132, 2002

0016-7037/02 $22.00 + .00

PII S0016-7037(00)00980-8

Dynamic processes occurring at the Cr^{III}_{aq}-manganite (γ-MnOOH) interface: Simultaneous adsorption, microprecipitation, oxidation/reduction, and dissolution

ROBERT M. WEAVER,[1,*] MICHAEL F. HOCHELLA, JR.,[1] and EUGENE S. ILTON[2]

[1]Nanogeoscience and Technology Laboratory, Department of Geological Sciences, Virginia Polytechnic Institute and State University, 4044 Derring Hall, Blacksburg, VA 24061, USA

[2]Lehigh University, Earth and Environmental Sciences Department, 31 Williams Drive, Lehigh University, Bethlehem, PA 18015-3188, USA

(*Received April* 2, 2001; *accepted in revised form May* 17, 2002)

Abstract—The complex interaction between Cr^{III}_{aq} and manganite (γ-MnOOH) was systematically studied at room temperature over a pH range of 3 to 6, and within a concentration range of 10^{-4} to 10^{-2} M $CrOH^{2+}_{aq}$. Solution compositional changes during batch reactions were characterized by inductively coupled plasma spectroscopy and ultraviolet-visible spectrophotometry. The manganites were characterized before and after reaction with X-ray photoelectron spectroscopy, scanning electron microscopy (SEM), high-resolution field-emission SEM, and energy-dispersive spectroscopy analysis. Fluid-cell atomic force microscopy was used to follow these metal-mineral interactions in situ. The reactions are characterized by (1) sorption of Cr^{III} and the surface-catalyzed microprecipitation of Cr^{III}-hydroxy hydrate on manganite surfaces, (2) the acidic dissolution of the manganite, and (3) the simultaneous reductive dissolution of manganite coupled with the oxidation of Cr^{III}_{aq} to highly toxic Cr^{VI}_{aq}. Cr^{III}-hydroxy hydrate was shown to precipitate on the manganite surface while still undersaturated in bulk solution. The rate of manganite dissolution increased with decreasing pH due both to acid-promoted and Mn-reduction-promoted dissolution. Cr oxidation also increased in the lower pH range, this as a result of its direct redox coupling with Mn reduction. Neither Mn^{II} nor Cr^{VI} were ever detected on manganite surfaces, even at the maximum rate of their generation. At the highest pHs of this study, Cr^{III}_{aq} was effectively removed from solution to form Cr^{III}-hydroxy hydrate on manganite surfaces and in the bulk solution, and manganite dissolution and Cr^{VI}_{aq} generation were minimized. All interface reactions described above were heterogeneous across the manganite surfaces. This heterogeneity is a direct result of the heterogeneous semiconducting nature of natural manganite crystals and is also an expression of the proximity effect, whereby redox processes on semiconducting surfaces are not limited to next nearest neighbor sites.

1. INTRODUCTION

In natural environments, manganese oxides are frequently recognized for their extraordinary sorption capacity and strong oxidizing ability (McKenzie, 1967, 1980; Murray et al., 1968; Chao and Anderson, 1974; Means et al., 1978; Burns and Burns, 1979; Murray and Dillard, 1979; Dillard et al., 1981; Hem et al., 1989; Fendorf et al., 1992). In addition, Mn-oxides have repeatedly been shown to be the only naturally occurring, inorganic phases capable of oxidizing Cr^{III}_{aq} (e.g., $CrOH^{2+}_{aq}$) to Cr^{VI}_{aq} species (e.g., $HCrO_4^-$, chromate) (Gray and Malati, 1979; Amacher and Baker, 1982; Eary and Rai, 1987; Fendorf and Zasoski, 1992). The potential for Cr^{III}_{aq} oxidation by Mn-oxides is of great concern not only because chromium is the most common, redox-active inorganic groundwater contaminant in the United States and several other industrialized countries, but also because Cr^{VI}_{aq} is more labile than Cr^{III}_{aq} and is carcinogenic even at low concentrations (e.g., $<$ 50 ppb; Nriagu and Nieboer, 1988; Kavanaugh, 1994).

The interaction between Cr^{III}_{aq} and Mn-oxides is complex not only because chromium uptake and oxidation occurs, but also because depending on the solution conditions, the Mn-oxide surface undergoes simultaneous reductive dissolution and acidic dissolution. Previous studies in this system have focused on Cr^{III}_{aq} oxidation kinetics by synthetic pyrolusite (b-MnO_2) (Eary and Rai, 1987), synthetic manganite (g-MnOOH) (Johnson and Xyla, 1991), synthetic birnessite (d-MnO_2) (Fendorf and Zasoski, 1992; Chung et al., 1994; Silvester et al., 1995; Chung, 1998), synthetic hausmannite (Mn_3O_4), and synthetic bixbyite (Mn_2O_3) (Rophael and Boulis, 1982; Malati and Rophael, 1999). Other Cr^{III}_{aq}-Mn-oxide studies have investigated: (1) the sorption and oxidation of Cr^{III}_{aq} with the concomitant solid state reduction of synthetic birnessite studied with X-ray photoelectron spectroscopy (XPS) (Banerjee and Nesbitt, 1999); (2) bulk atomic structural changes (e.g., bond length and angle) of synthetic birnessite accompanying reaction with Cr^{III}_{aq} studied by extended X-ray absorption fine structure (EXAFS) and X-ray absorption near edge spectroscopy (Manceau and Charlet, 1990), and (3) Cr^{III}_{aq} oxidation by synthetic d-MnO_2 as elucidated by high-resolution transmission electron microscopy, electron energy loss spectroscopy, and energy-dispersive spectroscopy (EDS) (Fendorf et al., 1992).

Even with this vast base of experimental observations, in situ microscopic observations at the Cr^{III}_{aq}–Mn-oxide interface are not available. Considering this gap, it was our primary goal to obtain such observations of the surface reactions. Of near equal importance was the need to measure how the composition of the Mn-oxide surface and the contacting aqueous solution changed during the reaction, and to do this using natural crystals. We chose to study Cr^{III}_{aq}-manganite interactions because

* Author to whom correspondence should be addressed, at The McCrone Research Institute, 2820 South Michigan Avenue,Chicago IL 60616-3292, USA (rweaver@mcri.org).

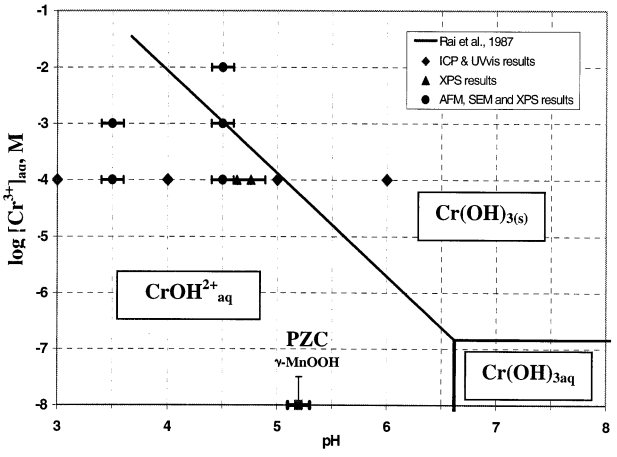

Fig. 1. Stability diagram for Cr^{III}_{aq} as a function of pH and $[Cr^{III}]_{aq}$ (modified after Rai et al., 1987). $CrOH^{2+}_{aq}$ is the dominant species under acidic conditions. The plotted data show the aqueous conditions employed in each of our experiments. The symbols indicate the primary analytical method or methods used to characterize that particular experiment as discussed in the results. The PZC of manganite has been labeled on the pH axis.

manganite, like other Mn^{3+}-oxides, such as feitknecktite (b-MnOOH) and hausmannite (Mn_3O_4), is a common intermediate product of Mn^{2+}_{aq} oxidation or $MnO_{\sim 2(s)}$ disproportionation (Hem, 1981; Hem et al., 1982; Murray et al., 1985; Lind, 1988; Junta and Hochella, 1994). Manganite was also chosen because it is one of the few Mn-oxides that naturally forms relatively large, cleavable crystals suitable for our instrumental methods.

To study this complex interaction, manganite cleavage surfaces and powders were reacted with Cr^{III}_{aq}, and the aqueous and solid products were analyzed via microscopies (atomic force microscopy [AFM], scanning electron microscopy [SEM]) and surface-sensitive and bulk spectroscopies [XPS, EDS], inductively coupled plasma spectroscopy [ICP] and ultraviolet-visible spectrophotometry [UVvis]). Fluid-cell AFM was used to observe the uptake of Cr and the dissolution of manganite in situ. The reacted surfaces were also examined by means of field-emission SEM (FESEM) at high resolution and low accelerating voltage, without applying a conductive coating. The bulk solution experiments were not intended to provide an exhaustive study of Cr^{III}_{aq} oxidation and manganite dissolution kinetics, but instead they provide background data to complement our microscale AFM, SEM, and XPS experiments. Finally, the local electronic behavior of the manganite cleavage surfaces before reaction were studied with scanning tunneling microscopy (STM).

Our experiments were conducted over a range of aqueous conditions for which the activity of Cr^{III}_{aq} was controlled primarily by the equilibrium between $CrOH^{2+}_{aq}$ and $Cr(OH)_3{\cdot}3H_2O_{(s)}$. This stability was studied in detail by Rai et al. (1987) and is generally described by Eqn. 1 and Fig. 1

$$CrOH^{2+}_{aq} + 5H_2O = Cr(OH)_3{\cdot}3H_2O_{(s)} + 2H^+ \qquad (1)$$

$$\log K = -5.78$$

(Note that although Rai et al. (1987) suggested that the Cr precipitate was amorphous $Cr(OH)_3$, we have found this phase to be crystalline $Cr(OH)_3 0.3H_2O$; see section 3.1 of this article). The points plotted in Fig. 1 show the solution conditions we employed in each of our experiments. As can be seen, with the exception of the one set of experiments performed in 10^{-2} M Cr^{III}_{aq}, all of the results presented were performed in 10^{-3} M or 10^{-4} M $CrOH^{2+}_{aq}$ and over a pH range of 3 to 6. Under these conditions, the saturation index (SI) for $Cr(OH)_3{\cdot}3H_2O$ ranges from -0.46 to 0.14. This SI range corresponds to $6000\times$ undersaturated to $600\times$ oversaturated with respect to $Cr(OH)_3{\cdot}3H_2O$. These solution conditions were not selected for the purpose of reproducing a specific Cr^{III}_{aq} waste environment, although conditions in this range do exist. The conditions were selected so that comparisons to existing data could be made; so that the Mn_{aq} and Cr_{aq} detection limit would not be an issue; and so that the reaction rates were in a range that was convenient for sampling.

2. MATERIALS AND METHODS

2.1. Manganite Characterization and Aqueous Solutions

The manganite (γ-MnOOH) samples used in this study were from Ilfeld, Germany, and Pawling Mine, New York (Virginia Polytechnic Institute Museum R706 and Ma5). Structural and chemical characterization with X-ray diffraction (XRD), XPS, EDS, and wavelength dispersive spectroscopy (WDS) (data not shown) confirmed the manganites to be highly crystalline with minor amounts (<1%) of Ca and Fe. Trace element chemistry was not investigated.

Samples for AFM, SEM, and STM observations/experiments were cleaved from larger manganite crystals with a pestle or scalpel. The resulting (010) and (110) surfaces were locally optically flat and often exhibited twinning. Although the surfaces were stable in air (as observed by AFM and XPS), it was standard practice to use freshly exposed surfaces (i.e., <1 d).

Fine-grained manganite was prepared by grinding samples in a McCrone micronizing mill (crushing action is primarily by shear stress) for 10 min. XRD patterns of the ground powder showed no loss in crystallinity. The surface area of the powder, as measured by N_2 BET, was 8.9 ± 0.1 m^2/g. A PZC of 5.4 ± 0.2 was determined from surface titrations conducted at five ionic strengths ranging from ~0 to 0.1 M $NaNO_3$.

All chemicals were of reagent grade or higher and solutions were prepared from distilled, deionized water obtained from a Millipore Synthesis A10 water system (18 MW, 1 ppb total organic carbon, ultraviolet light treated, ultrafiltration membrane, 0.2 mm filtered). All glassware and high-density polyethylene (HDPE) containers were rinsed with 0.01 M HNO_3 and water before use. Standardized Cr^{III}_{aq} solutions were prepared fresh (<12 h) for each experiment. All experiments were conducted at room temperature (23 ± 2°C), and solutions were assumed to be in equilibrium with air. Previous work has shown that Cr^{III}_{aq} is not significantly oxidized by O_2 even after 1 month (Schroeder and Lee, 1975; Van Der Weijden and Reith, 1982; Eary and Rai, 1987).

2.2. Batch Experiments for Aqueous Chemical Analysis by ICPand UVvis

Reactions were performed in Parafilm-covered, 500-mL HDPE containers in solutions held at a constant pH of 3, 4, 5, or 6 (±0.02) by automatic titration (Radiometer ABU 901 autoburette) of 0.1 mol/L HNO_3. Solutions were stirred vigorously (300 rpm) by an overhead Teflon paddle. Immediately before reaction, an aliquot of the manganite suspension and the Cr^{III}_{aq} stock solution was sampled to measure the initial concentrations of manganese and chromium. Reactions were initiated by adding pH-adjusted, 10^{-3} M $Cr(NO_3)_3{\cdot}6H_2O$ (17.77 mL) to 160 mL of the stirred preequilibrated manganite suspension. The final reacting solutions contained 10^{-4} M Cr^{III}_{aq}, 0.005 M $NaNO_3$, and 0.45 g/L manganite (~4.0 m^2/L). Samples were periodically extracted with a HDPE syringe, filtered through 0.2 mm nitrocellulose, analyzed

for Cr^{VI}_{aq} with UVvis, and then stored in capped HDPE containers to await ICP analysis.

Additional control experiments were performed to measure the extent of (1) sorption of chromium to the HDPE surfaces, (2) acidic dissolution of manganite, and (3) Cr^{III}_{aq} oxidation by Mn^{III}_{aq} in the absence of manganite. The extent of chromium uptake by HDPE over a 24-h period was found to be negligible. For the acidic dissolution study, the reacting solutions contained 0.005 M $NaNO_3$, 0.45 g g-MnOOH/L, were stirred vigorously (300 rpm) and held at pH 3, 3.5, 4, 5, and 6 $\pm$ 0.05 by automatic addition of 0.1 N HNO_3. Samples were collected after approximately 10 min, 1 h, and 8 h of reaction, centrifuged (2500 rpm), and filtered through 0.2-mm nitrocellulose. To measure the extent of Cr^{III}_{aq} oxidation by Mn^{III}_{aq}, a standardized Mn^{III}_{aq} stock solution was prepared by acidically dissolving manganite in 0.1 N HNO_3. The solution obtained was then titrated with NaOH to pH 3, centrifuged (3500 rpm), filtered two times through 0.1 mm nitrocellulose and Mn^T was measured by ICP. The resulting Mn^{III}_{aq} solution had an absorption maximum at 300 nm. The amount of chromate produced by reaction of this Mn^{III}_{aq} solution (0.5 mL, 9×10^{-4} M) with Cr^{III}_{aq} (0.5 mL, 3×10^{-4} M) at pH 3 for 32 h was found to be less than 2×10^{-7} M Cr^{VI}_{aq} (i.e., $< 1\%$). At these Cr^{III}_{aq} and Mn^{III}_{aq} concentrations, Cr^{VI}_{aq} was only produced at pH >3.5 and it was evident that Mn-oxide precipitation was occurring. For this reason it was concluded that the amount of Cr^{VI}_{aq} produced by the direct reaction between Mn^{III}_{aq} and Cr^{III}_{aq} was negligible (i.e., $<1\%$) compared with the amount produced by direct reaction at the Mn-oxide surface.

2.3. Batch Experiments for Surface Analysis by XPS

Manganite samples for XPS analysis were recovered from their respective reaction vessels by centrifugation and decantation rather than filtration, to avoid contamination and allow for near complete recovery of the solids. For these reasons reactions were carried out in 50 mL HDPE centrifuge tubes, which were rotated end over end ($\sim$60 rpm). The reacting solution contained 0.45 g γ-MnOOH/L ($\sim$4.0 m^2/L), 10^{-4} M $CrCl_3 \cdot 6H_2O$ and 0.005 mol/L NaCl. The manganite powder was preequilibrated in 0.005 mol/L NaCl electrolyte at pH 4.5 for 24 h. Reactions were initiated by the addition of 10 mL of pH 4.5, 2×10^{-4} M Cr^{III}_{aq} and continued for 3 min, 30 min, 8 h, and 20 h. Solution pH was maintained by manual addition of 0.05 mol/L HCl. For the 3 and 30 min experiments the pH did not exceed 4.61 and for the 8- and 20-h experiments the pH did not exceed 4.73. Reactions were ended by centrifugation (2500 rpm) and decantation of the supernate. The manganite powder was then shaken for 20 s. with 20 mL of pH 4.6 HCl, centrifuged and decanted. This rinsing process was performed five times, after which the manganite was dried under low vacuum (10^{-5} torr), dispersed onto a tin sheet with a razor, pressed and analyzed by XPS. The $Cr2p^{3/2}$ region was scanned first to minimize potential X-ray beam-induced reduction of Cr^{6+} (Halada and Clayton, 1991; Ilton et al., 1997).

2.4. In Situ Fluid-Cell AFMand Ex Situ SEMExperiments

Manganite cleavage fragments were mounted on Al or glass discs with a carbon-based adhesive (AFM fluid-cell experiments) or reacted without mounting (SEM experiments) in a HDPE container with 20 mL of standardized Cr^{III}_{aq} solution. We attempted to remove submicron cleavage fragments adhering to the surface with a high-velocity N_2 stream, sonification in pH 5.0 HNO_3, or both. However, we found that these cleaning procedures were not entirely effective, and furthermore, the particles did not significantly affect our observations. For this later reason, the surface cleaning steps were eventually deemed unnecessary. Before reaction, manganite surfaces were examined by Nomarski differential interference contrast microscopy and AFM to document surface features (e.g., microtopography, terrace roughness, twinning). Samples were then placed in the AFM fluid-cell or a HDPE container and reacted with Cr^{III}_{aq}.

For the AFM fluid-cell experiments, Corning vacuum grease was applied between the O-ring and the sample disk to prevent leaks and to minimize image distortion caused by friction between the O-ring and sample. When AFM images were not being obtained, the tip was lifted $\sim$50 mm from the sample surface (to not influence the reaction) and solution flow was resumed. Solutions were pumped at a speed of $\sim$0.4 mL/min (i.e., $\sim$1 cell volume flush every 10 s) through Pt-cured silicone tubing. In most of the AFM fluid-cell experiments, the manganite was first exposed to a HCl or HNO_3 solution to observe the process of acidic dissolution. These observations allowed us to be confident that the solution was free of particulate contaminants that might be mistaken for $Cr(OH)_3 \cdot 3H_2O$ precipitates. After observing the manganite surface under exposure to acid, the feed solution was switched to a 10^{-3} or 10^{-4} M $CrOH^{2+}_{aq}$ solution and AFM imaging was resumed. Upon removal from the AFM, the sample was dried in a high velocity N_2 stream and analyzed by XPS, SEM, EDS, or some combination of these. For XPS observations, the sample was remounted on a fresh aluminum- or carbon-coated (e.g., HOPG, carbon adhesive) surface. This remounting allowed us to be certain that the Cr and Mn XPS signals were originating from the manganite with no contribution from the sample holder.

2.5. Scanning Probe Microscopy

AFM images were collected with a Digital Instruments Nanoscope IIIa Multimode atomic force microscope, operating in either air or aqueous solution, and in contact or Tapping mode (TMAFM). The XY scale was calibrated with a 1-mm standard, and the Z scale was calibrated against the basal spacing of mica (i.e., 0.995 nm). AFM probes used have a Si tip (nominal radius $\sim$20 nm) on a 100-mm SiN_3 cantilever. The acrylic AFM fluid-cell holds $\sim$0.03 to 0.07 mL, depending on the sample size and the degree of silicone O-ring compression (see Johnsson et al., 1991, for cell schematic).

A Digital Instruments scanning tunneling microscope was used to characterize the local electronic behavior of manganite. Although a wide range of bias voltages and set point currents were tried, and it was possible in some tip-sample approaches to establish a tunneling current, the current was too unstable during scanning for good surface imaging. The implications of this observation to surface reactivity are significant and will be discussed later.

2.6. Electron Microscopy and Spectroscopy

SEM images, EDS spectra, and WDS spectra were collected by three different instruments: a LEO 1550 field-emission scanning electron microscope with IXRF energy-dispersive spectroscope, a Camscan Series II scanning electron microscope, and a Cameca SX50 electron microprobe. Pertinent imaging conditions are reported in the figure captions. The FESEM images were collected at voltages as low as 1 kV with an in-lens secondary electron detector. Under these conditions, the lateral resolution and surface sensitivity are superior as a result of enhancement of the SE_I signal (Goldstein et al., 1992). SEM imaging was also performed by varying the accelerating voltage to obtain voltage contrast SEM images. Voltage contrast images showed the extent of heterogeneous electrical conduction in the sample, an important sample property discussed later.

2.7. XPS

XPS spectra were collected with a Scienta ESCA-300 and a Perkin-Elmer 5400. The Scienta XPS utilized monochromatic Al-Ka X-rays, generated at a power of 1.9 kW, and had an analysis area of 1.0 cm $\times$ 300 mm. Photoelectrons were collected from a 90° take-off angle and the energy analyzed via a pass energy of 150 eV. Survey scans were collected with a 0.5-eV step size and narrow scans with a 0.1- or 0.05-eV step size. Because manganite is a wide band gap semiconductor, it was necessary to use a flood gun to neutralize the charge that developed on the sample during irradiation. XPS spectra collected with the Perkin Elmer XPS used nonmonochromatic Al-Ka X-rays and a spot size of either 1.1 mm^2 or a diameter of 600 mm. Survey and regional scans were collected with pass energies of 44.8 and 17.9 eV, respectively. Analyses were performed in both instruments at pressures of less than 4×10^{-8} torr. XPS spectra were charge referenced to adventitious carbon at 284.6 eV. Peak fitting of photolines was performed with a Shirley background correction and Voigt (gaussian-Lorentzian) curve-fitting function.

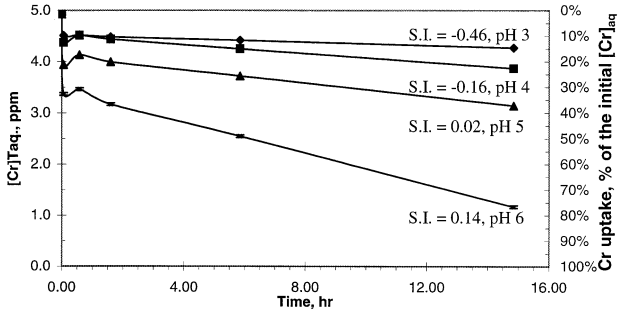

Fig. 2. Total aqueous chromium concentration with time and pH as measured by ICP. The initial solution contained 10^{-4} M Cr^{III}_{aq} (4.9 ppm) and 0.45g/L γ-MnOOH at pH 3, 4, 5, and 6. The decreasing trend in the total aqueous chromium with time and pH results from $Cr(OH)_3{\cdot}3H_2O$ precipitation and Cr-adsorption on the manganite surface and in solution. On the right side y-axis is given the Cr uptake as a percentage of the initial chromium concentration. SI = saturation index for $Cr(OH)_{3(s)}$.

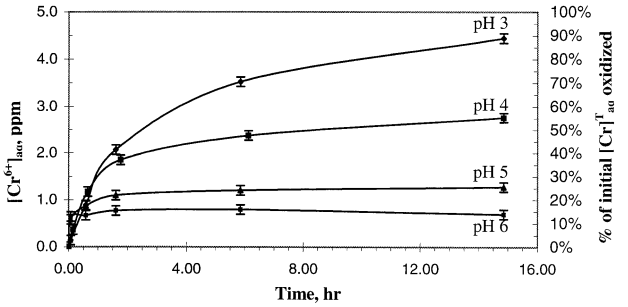

Fig. 3. Chromate concentration with time and pH as measured by UVvis. The initial $[Cr^{III}]_{aq}$ was 4.9 ppm ($\sim 10^{-4}$ M). The y-axis on the right side indicates the percentage of the initial Cr^{III}_{aq} that has been oxidized to $HCrO_4^-$.

2.8. UVvis Spectrophotometry

A Beckman Coulter DU640 spectrophotometer was used to record wavelength scans. Solutions were analyzed in a 1-cm path length, quartz or methacrylate cuvet. The measured absorbance for chromate was standardized against known concentrations of analytic-grade Cr^{VI}_{aq}, adjusted to pH. Beer's Law behavior was observed for the concentration range measured (Buerge and Hug, 1999). A precision on replicate samples of $\pm$12 ppb was assigned to all peaks.

2.9. ICP

Aqueous concentrations for Cr and Mn were measured on a Spectro Analytical Instruments SpectroFlame ICP. Cr and Mn standards were prepared from Plasma-pure–grade reagents diluted with the matrix used in each experiment. Reported ICP measurements are the average of three measurements. A precision of $\pm$20 ppb was observed in replicate measurements.

3. RESULTS

3.1. Solution Compositions with Time and pH

The uptake and oxidation of chromium and the dissolution of manganite was observed over a 15-h period and pH range from 3 to 6. Within the first several minutes of each reaction, a substantial portion of the total chromium uptake had already occurred (Fig. 2). However, after an additional 30 min, a small amount (0.2 to 3.9%) of the chromium was released back into solution. In general, the amount of chromium removed from solution was greatest for the higher pH experiments. For example, after 15 h of reaction at pH 3, approximately 13% of the initial total aqueous chromium ($[Cr]^T_{aq}$) was removed from solution, whereas at pH 6, over the same 15-h period, $\sim$76% of the initial $[Cr]^T_{aq}$ was removed. The most substantial change in chromium uptake occurred between pH 5 and 6, when the solution became supersaturated with respect to $Cr(OH)_3{\cdot}3H_2O$ and bulk precipitation occurred. The bulk precipitate was identified by XRD, as $Cr(OH)_3{\cdot}3H_2O$ (JCPDS 16-817) in separate experiments conducted at pH 6.5, 10^{-4} M and pH 4.5, 10^{-2} M Cr^{III}_{aq} in the absence of manganite. The solubility data of Eary and Rai (1987) were used to calculate that $Cr(OH)_3{\cdot}3H_2O_{(s)}$ saturation occurs at pH 4.9 for a 10^{-4} M $CrOH^{2+}$ solution (see Eqn. 1). By use of this $Cr(OH)_3{\cdot}3H_2O_{(s)}$ stability data, we can attribute, to at least a first approximation, chromium uptake at pH $>$ 4.9 to $Cr(OH)_3{\cdot}3H_2O_{(s)}$ precipitation and at pH $<$ 4.9 to chromium adsorption or surface catalyzed precipitation.

Accompanying the removal of chromium from solution is the oxidation of Cr^{III}_{aq} to Cr^{VI}_{aq}. The production of Cr^{VI}_{aq} is initially very rapid and nonlinear for all pHs, but eventually slows and approaches linearity (Fig. 3). The conversion is most efficient at lower pHs. For example, at pH 3, 90% of the initial $[Cr]^T_{aq}$ is oxidized to Cr^{VI}_{aq} within $\sim$15 h, whereas at pH 6, only 14% of the initial $[Cr]^T_{aq}$ was oxidized to Cr^{VI}_{aq} after 15 h. By comparing the $[Cr^{VI}]_{aq}$ to that of $[Cr]^T_{aq}$ after 15 h of reaction at pH 3, it was found that the reaction at pH 3 had reached completion (i.e., $[Cr^{VI}]_{aq} = [Cr]^T_{aq}$ after 15 h), whereas at pH 4, 5, and 6 after 15 h of reaction approximately 72%, 41 and 59% of the $[Cr]^T_{aq}$ occurs as Cr^{VI}_{aq}. The percentage at pH 6 increases to 59% as a result of $Cr(OH)_3{\cdot}3H_2O_{(s)}$ precipitation.

The amount of manganite dissolution by simultaneous reductive dissolution and acidic dissolution is greatest at pH 3 (Fig. 4). Fig. 4 also shows the change in the total aqueous manganese, with time and pH, caused by acidic dissolution alone. It can be seen that at pH 3 the rate of acidic dissolution exceeds that for acidic plus reductive dissolution. However, at pH 4, the rate of acidic dissolution is less than the rate of acidic plus reductive dissolution. This behavior demonstrates that for pHs less than $\sim$3.5, chromium inhibits the rate of manganite dissolution relative to chromium-free solutions. A similar inhibition of the dissolution rate by chromium was observed by Banerjee and Nesbitt (1999) for δ-MnO_2 at pH 4.6. However, Eary and Rai (1987) observed that for β-MnO_2 the rates of acidic dissolution and reductive plus acidic dissolution were approximately the same at pH 4, but the rate of reductive plus acidic dissolution was faster at pH 3. In Fig. 4, the reductive plus acidic dissolution curves have an initial period of nonlinearity (recall, so did the chromate curves, Fig. 3, whereas the acidic dissolution curves are linear with time after just a few minutes. Comparing the results of Figures 3 and 4 for the first 6 h of reaction, the $[Mn]^T_{aq}$:$[Cr^{VI}]_{aq}$ ratio can be shown decrease with increasing pH, from 4.3 at pH 3, 3.7 at pH 4, 3.0 at pH 5 and 2.1 at pH 6. The significance of this ratio for judging changes in the overall reaction stoichiometry with pH and time are discussed later.

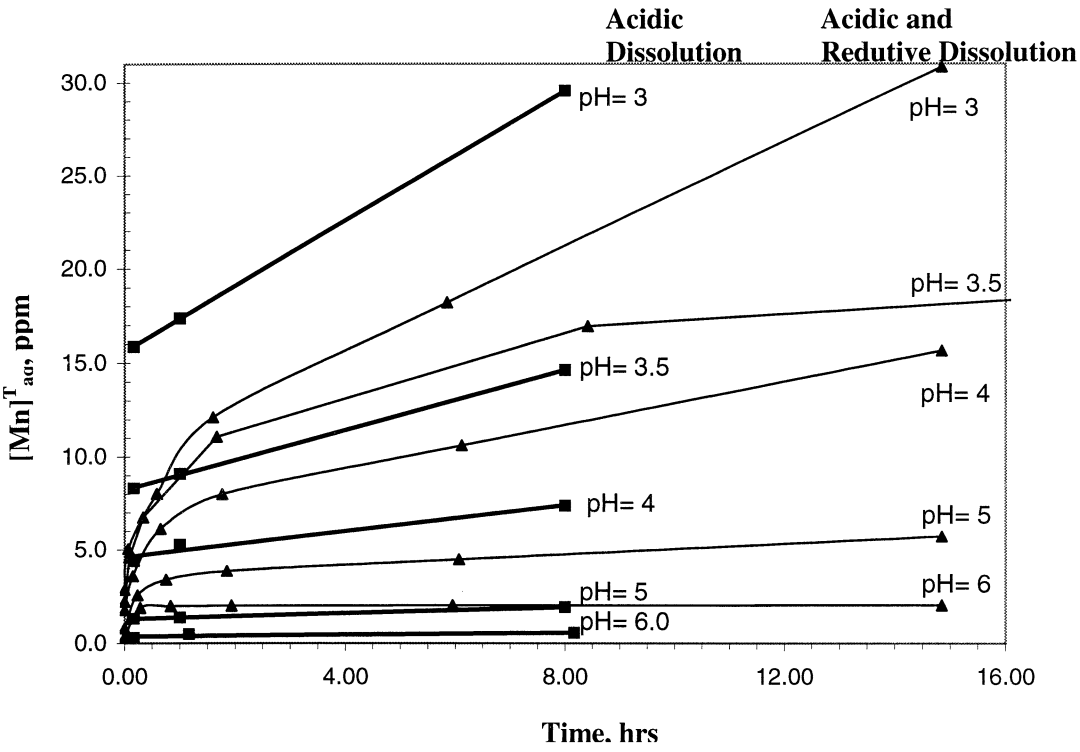

Fig. 4. Total aqueous manganese concentration with reaction time and pH as observed for acidic dissolution in HNO_3 (values plotted to 8 h) and for reductive plus acidic dissolution in 4.9 ppm ($\sim 10^{-4}$ M) Cr^{III}_{aq} (values plotted to 15 h.). Note that at pH 3.5, the rate of acidic dissolution is nearly the same as the rate of reductive plus acidic dissolution. However, at pH 3, the rate of acidic dissolution is greater, and for pH $>$ 3.5, the rate of reductive plus acidic dissolution is greater. In the acidic dissolution experiments, the first sample was collected after 10 min of reaction.

3.2. Surface Compositions with Time

XPS spectra obtained from manganite powders reacted with Cr^{III}_{aq} (Fig. 5) show an increase in surface bound chromium with reaction time, as was suggested by the solution data (see Fig. 2). The concentrations of surface chromium relative to surface manganese (as determined from ratios of $Cr2p^{3/2}$: $Mn2p^{3/2}$ photopeak areas) increases with reaction time up to the 8-h sample, then does not change for the sample reacted for 20 h. This increase in surface bound chromium suggests that surface saturation with respect to chromium is reached in less than 8 h. However, this disagrees with the solution data for $[Cr]^{T}_{aq}$ with time (Fig. 2), which suggest that at pH 4.5 Cr uptake occurs throughout the reaction period. The reason for this discrepancy between the Cr-aqueous and Cr-solid concentration profiles is not known, but there are at least two possibilities: first, Cr could be taken up on rough surfaces, not all portions of which are visible to the electron energy analyzer of the XPS instrument; and second, the rinsing procedures used for the XPS samples, which could have removed some of the adsorbed Cr or $Cr(OH)_3{\cdot}3H_2O_{(s)}$ surface precipitate.

The oxidation state of surface bound chromium was determined to be Cr^{3+} on the basis of three lines of XPS evidence, as follows. (1) The magnitude of the Cr2p spin orbit splitting is 9.8 $\pm$ 0.1 eV. Reported values for Cr2p splitting of Cr^{3+} compounds (e.g., Cr_2O_3, CrOOH and $Cr(OH)_3{\cdot}0.4H_2O$) are 9.7 to 9.8 eV, whereas splitting for Cr^{6+} compounds (e.g., CrO_3, Na_2CrO_4, $K_2Cr_2O_7$) are 9.2 to 9.3 eV (Ikemoto et al., 1976; Halada and Clayton, 1991). (2) The binding energy of the $Cr2p^{3/2}$ photopeak at 576.7 $\pm$ 0.1 eV is consistent with reported values for Cr_2O_3, CrOOH and $Cr(OH)_3{\cdot}0.4H_2O$, which range from 576.45 to 577.00 eV (Fig. 6). Compounds containing Cr^{6+} have binding energies of 578.3 to 579.8 eV, respectively (Banerjee and Nesbitt, 1999 and references therein for $Cr^{3+,\ 4+,\ 5+,\ 6+}$ binding energies). (3) Our raw data are in good agreement with a $Cr2p^{3/2}$ peak modeled when the theoretical multiplet structure of the Cr^{3+} free ion calculated by Gupta and Sen (1974, 1975) are used (Fig. 6, Table 1).

Surface manganese was determined to be Mn^{3+} in all reacted samples on the basis of three lines of evidence, as follows. (1) The Mn3s multiplet splitting of 5.5 $\pm$ 0.1 eV observed for each reaction period is diagnostic of Mn^{3+} (Fig. 7). The multiplet splitting for Mn^{4+} and Mn^{2+} are 4.5 eV and 6.2 eV, respectively (Evans and Raftery, 1982; Junta and Hochella, 1994). (2) The agreement of the $Mn2p^{3/2}$ photopeak shape with a theoretical model $Mn2p^{3/2}$ photopeak generated by the Mn^{3+} multiplets (slightly modified) calculated by Gupta and Sen (1974, 1975) (Fig. 8, Table 1) . (3) The $Mn2p^{3/2}$ peak position at 641.4 $\pm$ 0.1 eV approximates that reported for other Mn^{3+}-oxides (641.7 to 641.9 eV). $Mn2p^{3/2}$ peak positions for $Mn^{4+}O_2$ range from 641.9 to 642.6 eV and Mn^{2+} peak positions range from 640.4 eV to 641.7 (Junta and Hochella, 1994; Banerjee and Nesbitt, 1999).

Oxygen (O1s) XPS spectra show that with increased reaction time, the manganite surface becomes more enriched in OH^-

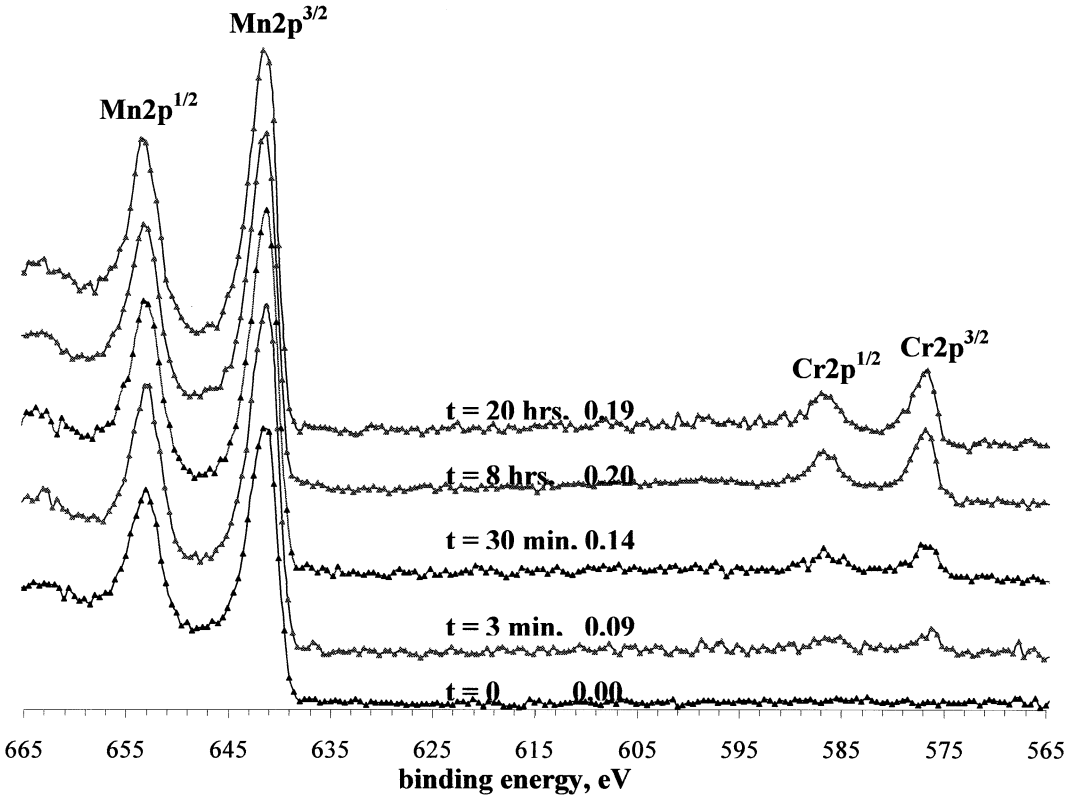

Fig. 5. XPS spectra of the Mn2p and Cr2p photopeaks of manganite before and after exposure to pH ~4.6, 10^{-4} M Cr^{III}_{aq} solution for the lengths of time indicated on each spectra. The number following the reaction time is the ratio of the $Cr2p^{3/2}$: $Mn2p^{3/2}$ peak areas.

and H_2O relative to O^{2-} (Fig. 9). This increase in OH^- and H_2O correlates with the previously observed increase in chromium with reaction time (Fig. 5) and thus suggests that $Cr(OH)_3{\cdot}3H_2O$ is present at the surface. A control sample, reacted in pH 4.5 HCl for 30 min and no Cr^{III}_{aq}, still contained 1:1 (i.e., stoichiometric) quantities of O^{2-} and OH^- with a minor (~12%) amount of adsorbed water (see t = 0 in Fig. 9 and Table 1). This result strongly suggests that changes in the O1s spectra with time are attributable to reaction with aqueous chromium.

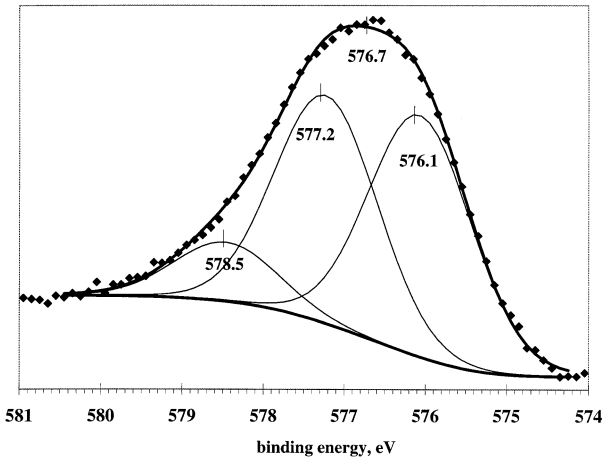

Fig. 6. XPS spectra of the $Cr2p^{3/2}$ photopeak collected after 20 h of reaction with pH ~4.6, 10^{-4} M Cr^{III}_{aq}. The peak shape and position in the spectra is nearly identical to that observed in the other samples. The three thin curves show the theoretical multiplet structure (slightly modified) calculated for the Cr^{3+} free ion (Gupta and Sen, 1974, 1975). The two thick, solid lines illustrate the fit to the raw data and the Shirley background.

3.3. Microscopic Observations of Reacted Surfaces

AFM and SEM images of reacted surfaces indicated that both chromium uptake and manganite dissolution could occur over a range of solution conditions (e.g., pH, $Cr(OH)_3{\cdot}3H_2O_{(s)}$-saturation) and were spatially heterogeneous (Figs. 10 to 14). The images also showed that the extent of Cr uptake and manganite dissolution were generally related to the degree of $Cr(OH)_3{\cdot}3H_2O$ saturation and pH, as would be expected given the solubility behaviors of $Cr(OH)_3{\cdot}3H_2O$ and manganite. Visual evidence of significant increases in the extent of Cr uptake was commonly observed in these images when the $Cr(OH)_3{\cdot}3H_2O$ SI was increased from −0.29 to 0.08 (Figs. 10, 11, 12). However, although the results of the batch reactor experiments demonstrated that minor Cr uptake does occur at low $Cr(OH)_3{\cdot}3H_2O$ saturations (Fig. 2), Cr uptake was not commonly observed under these conditions in the AFM experiments. When Cr-precipitates were observed in undersaturated solutions (e.g., SI −0.29, pH 3.5 10^{-4} M Cr^{III}_{aq}), they formed

Table 1. XPS peak parameters for $Mn2p^{3/2}$, $Cr2p^{3/2}$ and O1s.

Multiplet	BE (eV)	Intensity[a]	FWHM	G./L.[b]	Reference[c]
Mn^{3+}, $Mn2p^{3/2}$ 1	640.28	0.760	1.25	0.85	1
Mn^{3+}, $Mn2p^{3/2}$ 2	641.12	1.000	1.25	0.85	1
Mn^{3+}, $Mn2p^{3/2}$ 3	641.97	0.849	1.25	0.85	1
Mn^{3+}, $Mn2p^{3/2}$ 4	642.91	0.464	1.25	0.85	1
Mn^{3+}, $Mn2p^{3/2}$ 5	644.00	0.222	1.7	0.85	1
$Mn2p^{3/2}$ overall	641.40	1.33	~3.23	NA	1
Mn^{3+}, $Mn2p^{3/2}$ 1[e]	640.70	0.741	1.00	1.00	2,3
Mn^{3+}, $Mn2p^{3/2}$ 2[e]	641.40	0.741	1.00	1.00	2,3
Mn^{3+}, $Mn2p^{3/2}$ 3[e]	642.30	1.000	1.00	1.00	2,3
Mn^{3+}, $Mn2p^{3/2}$ 4[e]	643.10	0.519	1.00	1.00	2,3
Mn^{3+}, $Mn2p^{3/2}$ 5[e]	644.90	0.222	1.00	1.00	2,3
Cr^{3+}, $Cr2p^{3/2}$ 1	576.07	1.000	1.50	0.95	1
Cr^{3+}, $Cr2p^{3/2}$ 2	577.23	0.943	1.50	0.95	1
Cr^{3+}, $Cr2p^{3/2}$ 3	578.46	0.245	1.50	0.95	1
$Cr2p^{3/2}$ overall	576.70	1.48	~2.7	NA	1
Cr^{3+}, $Cr2p^{3/2}$ 1[de]	576.30	NA	1.00	1.00	2,3
Cr^{3+}, $Cr2p^{3/2}$ 2[de]	577.60	NA	1.00	1.00	2,3
Cr^{3+}, $Cr2p^{3/2}$ 3[de]	578.90	NA	1.00	1.00	2,3
Cr^{3+}, $Cr2p^{3/2}$ 1	576.02	NA	1.40	NA	4
Cr^{3+}, $Cr2p^{3/2}$ 2	577.00	NA	1.40	NA	4
Cr^{3+}, $Cr2p^{3/2}$ 3	577.79	NA	1.40	NA	4
O^{2-}, O1s	529.05	1.000	1.51	1.00	1, 3, 5
OH^{-}, O1s	530.40	1.000	1.51	1.00	1, 3, 5
H_2O, O1s	531.82	0.244	1.75	1.00	1, 3, 5

[a] Peak intensities are ratios against the most intense multiplet observed within each data set.
[b] Gaussian equals 1, Laurentzian equals 0.
[c] References: 1. This work; 2. Gupta and Sen (1975); 3. Nesbitt and Banerjee (1998); 4. Pratt and McIntyre (1996); 5. Junta and Hochella (1994).
[d] Peak parameters obtained from curve fitting of a scanned image of Figure 2 of Gupta and Sen (1975).
[e] Multiplet parameters are for the Cr^{3+} and Mn^{3+} free ion.

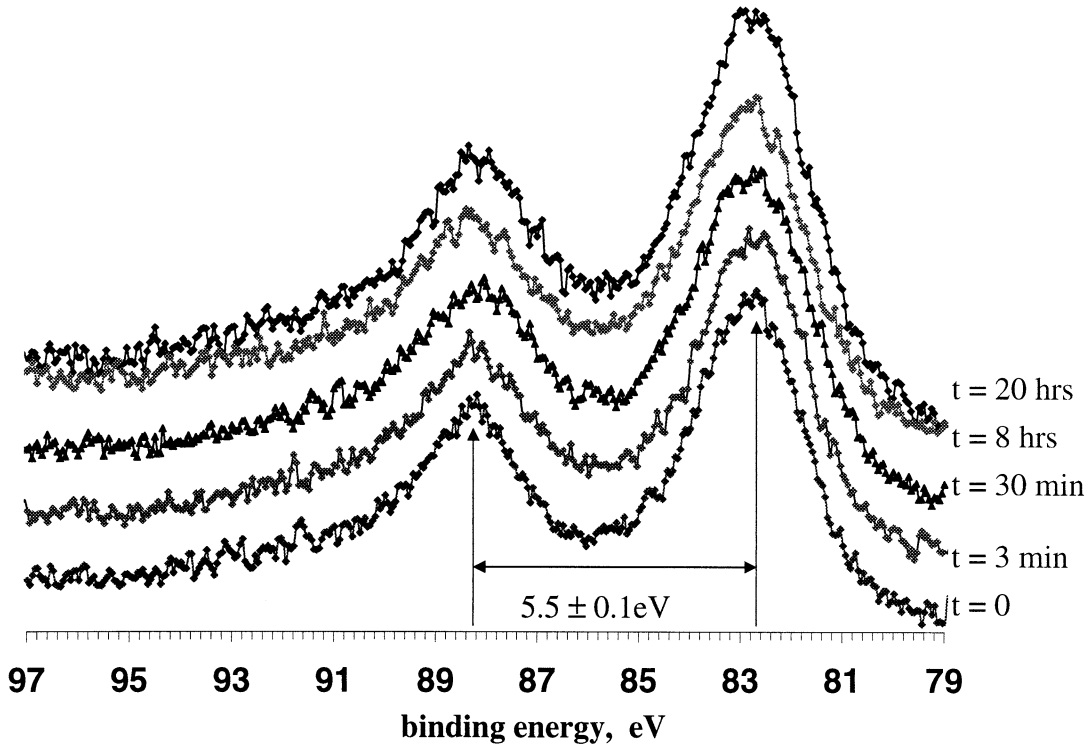

Fig. 7. Comparison of Mn3s XPS spectra of manganite before and after reaction with pH ~4.6, 10^{-4} M Cr^{III}_{aq}. The multiplet splitting of 5.5 ± 0.1 eV is constant throughout the reaction, indicating only the presence of Mn^{3+}.

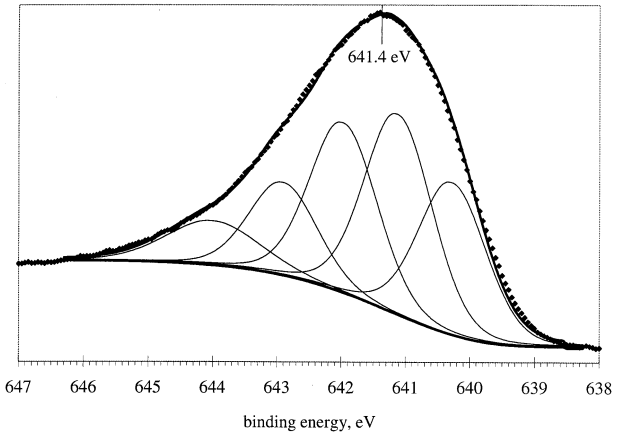

Fig. 8. XPS spectra of the $Mn2p^{3/2}$ photopeak collected after 8 h of reaction with pH ~4.6, 10^{-4} M Cr^{III}_{aq}. The position and shape of the $Mn2p^{3/2}$ peak was nearly identical for each reacted sample. The thin lines show the theoretical multiplet structure (slightly modified) of the Mn^{3+} free ion (Gupta and Sen, 1974, 1975). The bold line nearly superimposed on the raw data illustrates the good agreement between the theoretical model and experimental data.

immediately after exposure to Cr^{III}_{aq} and resembled those shown in Fig. 10b, measuring 20 to 80 nm wide and <1.5 nm high. Interestingly, there is no dissolution in this area, and no additional chromium uptake or release was observed over an additional 2-h period. At these conditions, it was also common to see rapid homogeneous dissolution with no evidence of chromium binding, and no change in the appearance of the surface.

Under solution conditions closer to $Cr(OH)_3{\cdot}3H_2O$ saturation (SI = −0.06, pH 4.5, 10^{-4} M Cr^{III}_{aq}) Cr uptake is generally more commonly observed and manganite dissolution is less apparent (Fig. 11). After exposure to Cr^{III}_{aq} for 5 min (Fig. 11b), $Cr(OH)_3{\cdot}3H_2O$ precipitates measuring from 10 to

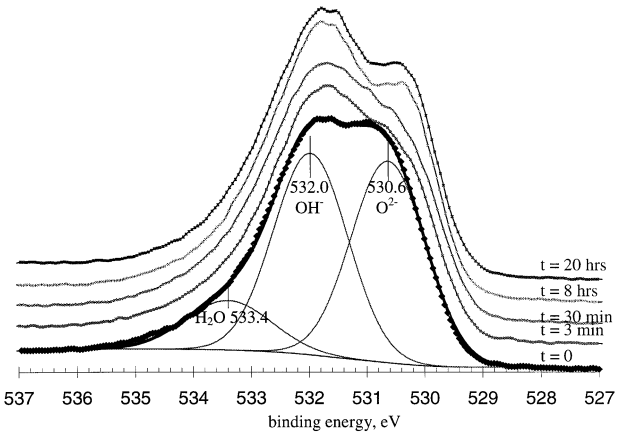

Fig. 9. XPS spectra of the O1s region on manganite before and after reaction with pH ~4.6, 10^{-4} M Cr^{III}_{aq}. The t = 0 sample was equilibrated in pH 4.5 HNO_3 for 30 min and is well fit (solid line superimposed on raw data) by using 1:1 quantities (i.e., stoichiometric) of OH^- and O^{2-} and minor (12%) H_2O. With increasing time of reaction, the contributions from the OH^- and H_2O components increase.

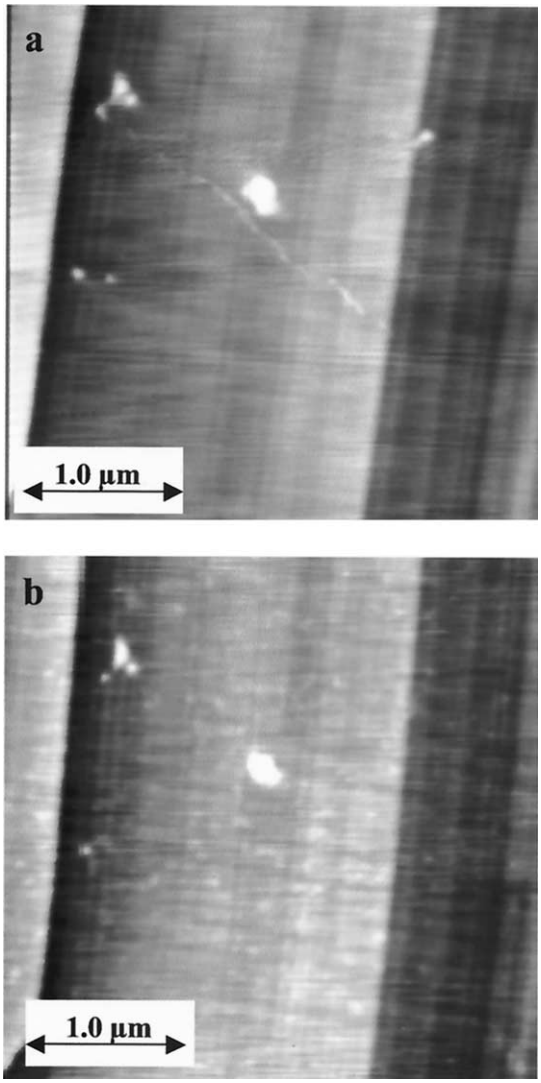

Fig. 10. Comparison of fluid-cell TMAFM images obtained in pH 3.5 HNO_3 (a, t = 0) and immediately after exposure (b, t = 4 min) to pH 3.5, 10^{-4} M $Cr^{III}_{aq.}$ The adsorbates/microprecipitates seen in (b) range from 0.3 to 1.3 nm tall and have lateral dimensions ranging from 10 to 100 nm. The lateral dimensions of these particles are likely to be much smaller, but the finite AFM tip radius (>20 nm) causes the particles to appear larger. In (b), a low-pass filter has been applied to remove a high-frequency component caused by the Tapping process.

200 nm wide and 0.3 to 10 nm high are visible, as is fine-scale surface pitting. Similar observations of heterogeneous precipitation and dissolution are seen by FESEM on other samples (Figs. 11c, d) However, it is also apparent that much of the surface has undergone little to no change. Incidentally, the precipitates seen in Fig. 11c,d were barely visible at 15 kV or when viewed with the conventional Everhart-Thornley SE_{II} detector.

Fig. 12 illustrates the degree of dissolution heterogeneity that was commonly seen in our experiments. The lower left area of Fig. 12a shows only a few dissolution pits, whereas the lower right area shows abundant pitting on the terraces and the upper central area (enlarged in Fig. 12b) shows extensive dissolution on the terraces and at step edges. There does not appear to be

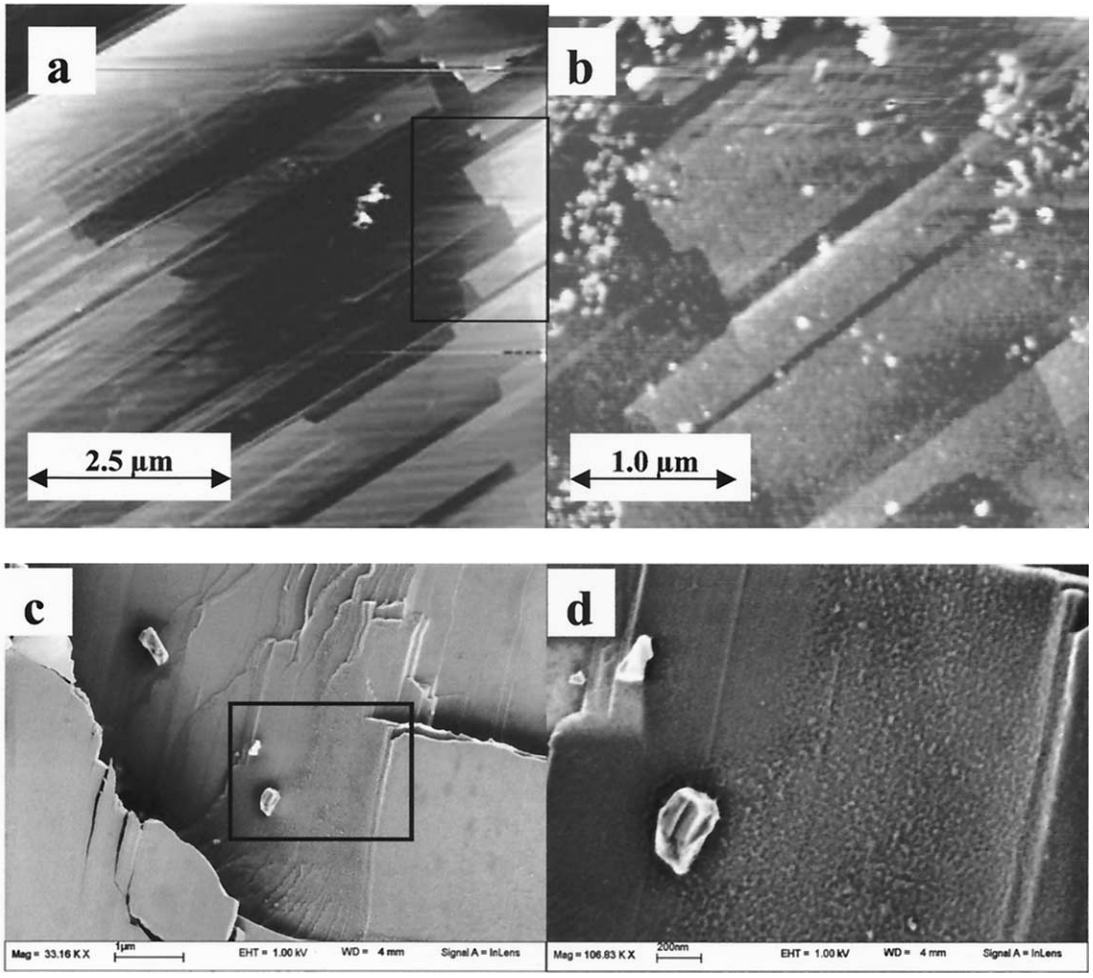

Fig. 11. AFM and FESEM images of manganite before (a) and after (b–d) exposure to Cr^{III}_{aq}. (a) TMAFM images obtained in pH 4.5 HNO_3 (t = 0). The fresh surface is characterized by broad atomically flat terraces with most step edges directed along [001]. (b) Area outlined in (a) after exposure to a pH 4.5, 10^{-4} M Cr^{III}_{aq} for 5 min. Compared with (a), the surface is rougher, with microprecipitates ranging in size from 0.3 to 10 nm tall and having lateral dimensions ranging from 10 to 300 nm. Fine-scale homogeneous surface pitting has also occurred. Adjacent areas may show dissolution with no precipitation or no change in the topography relative to the HNO_3^--reacted surface. (c, d) FESEM images of a different manganite sample after 2 h of exposure to pH 4.5, 10^{-4} M Cr^{III}_{aq} solution. The outlined area in (c) shows the location of (d). Images were obtained at 1 kV by using an in-lens SE_I detector. The distribution of adsorbates/microprecipitates is spatially heterogeneous. That is, patches of precipitate are bounded by large areas devoid of Cr-hydroxy hydrate precipitates. Chromium was detected on these samples by XPS but not by EDS.

any microprecipitates in this area, but the 30 kV accelerating voltage used for these images results in a low degree of surface sensitivity (Goldstein et al., 1992).

The AFM image sequence shown in Fig. 13 shows manganite dissolution and the development of microprecipitates within 4 min of exposure to a pH 4.5, 10^{-2} M Cr^{III}_{aq} (SI= 0.08) solution. Dissolution pits are elongated along [001] and measure ~40 nm wide, ~150 nm long and ~1 nm deep. The dissolution pits are slightly wider and deeper along the step edge (Fig. 13c), possibly due to defects generated here during cleavage. Also seen are new topographic highs (bright patches) corresponding to $Cr(OH)_3{\cdot}3H_2O$ precipitates measuring ~7 nm tall. The sample was then removed from the fluid-cell and reacted for 10 h in 20 mL of the same solution, after which the sample was imaged by AFM in air (Fig. 13d). The surface is now covered by microprecipitates, the tallest measuring ~50 nm. XPS analyses of the manganites shown in Figures 10 , 11, and 13 showed small to undetectable quantities of chromium with a $Cr2p^{3/2}$ binding energy of 576.6 ± 0.1 eV, indicative of Cr^{3+}.

The acidic dissolution of manganite was found to be less spatially heterogeneous than dissolution in the presence of chromium (that is, reductive plus acidic dissolution). Fig. 14 shows a series of AFM images obtained over a 1-h period during exposure to pH 3.5 HNO_3 in the absence of Cr^{III}_{aq}. Before reaction (Fig. 14a), the surface contains several steps bounding atomically flat terraces. Within 13 min of exposure, the terraces become riddled with randomly shaped, monolayer, deep (~0.5 nm) dissolution pits (Fig. 14b). Dissolution was initially most rapid at the step edges, as evidenced by the more expansive pits formed there. Although this seems to be the case, it is interesting to note that some sites along step edges

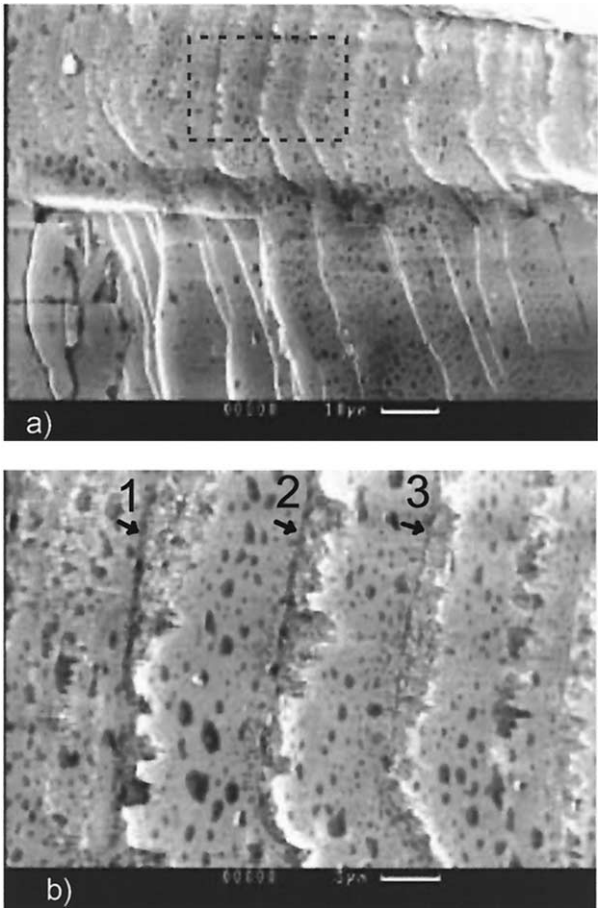

Fig. 12. SEM images of a manganite after reaction for 10 h in a pH 4.5 ± 0.2, ~10^{-3} M (46 ppm) Cr^{III}_{aq} solution. (a) Degree of dissolution heterogeneity commonly seen in our experiments. The extent of dissolution observed across the surface varies widely, with few dissolution pits seen in the lower left area relative to the area outlined above. (b) Enlargement of area outlined in (a). No Cr microprecipitates were observed in this area, although the 30-kV accelerating voltage used to collect these images results in a low degree of surface sensitivity. The linear dissolution features marked "1," "2," and "3" presumably mark the location of the step edges before dissolution.

(marked by arrows) undergo little dissolution. With continued reaction, dissolution proceeds primarily at step edges causing the existing pits to become broader and eventually coalesce (Fig. 14c,d). Tip-enhanced dissolution during a previous 1 × 1 μm scan is evidenced in Fig. 14d by the 1 μm^2 area near the center of the image. Subsequent 5-μm and 10-μm images collected after Fig. 14d showed that tip-enhanced dissolution in the 2.5-μm scan region of Fig. 14d was minor.

4. DISCUSSION

4.1. Aqueous and Surface Chemistry

The changes observed in the composition of the aqueous solution (i.e., $[Cr]^T_{aq}$, $[Mn]^T_{aq}$, $[Cr^{VI}]_{aq}$; Figs. 2 to 4) are generally interpretable on the basis of the solubility behaviors of $Cr(OH)_3{\cdot}3H_2O$ and manganite as a function of pH and redox state. Although both manganite and $Cr(OH)_3{\cdot}3H_2O$ are solubilized under acidic conditions, manganite is solubilized by reduction and $Cr(OH)_3{\cdot}3H_2O$ is solubilized by oxidation. These differences and similarities in the solubility behaviors may account for the observed trends in the concentrations of $Cr(OH)_3{\cdot}3H_2O_{(s)}$, Cr^{VI}_{aq}, Cr^{III}_{aq}, and Mn^T_{aq}. With decreasing pH the rate of manganite dissolution increases as a result of proton promoted dissolution (Eqn. 2) and also as a result of an increase in the rate of reductive dissolution (Eqn. 3). Although it is clear from our control experiments (see section 2.2) that Mn^{III}_{aq} is not a significant oxidant of Cr^{III}_{aq} when in the absence of manganite, Mn^{III}_{aq} may be capable of oxidizing Cr^{III}_{aq} to Cr^{VI}_{aq} when in the presence of manganite (Eqn. 4).

$$\gamma\text{-MnOOH} + 3H^+ = Mn^{3+}_{aq} + 2H_2O \quad (2)$$

$$CrOH^{2+}_{aq} + 3\gamma\text{-MnOOH} = HCrO^-_{4\,aq} + 3\,Mn^{2+}_{aq} + 3OH^- \quad (3)$$

$$CrOH^{2+}_{aq} + 3Mn^{3+}_{aq} + 3OH^- + \gamma\text{-MnOOH} = HCrO^-_{4\,aq} + 3Mn^{2+}_{aq} + 3H^+ + \gamma\text{-MnOOH}. \quad (4)$$

Slight to significant amounts of Cr uptake occurred over the pH range studied. Our observations show that for conditions of $Cr(OH)_3{\cdot}3H_2O$ oversaturation, uptake is due to $Cr(OH)_3{\cdot}3H_2O$ precipitation (Eqn. 1). For undersaturated conditions Cr uptake is due to Cr adsorption (Eqn. 5), where S indicates surface site and/or surface catalyzed precipitation of $Cr(OH)_3{\cdot}3H_2O$.

$$CrOH^{2+}_{aq} + \text{S-MnOOH} = Cr^{3+}\text{-MnOOH} + OH^- \quad (5)$$

We attempted to evaluate the contributions of acidic and reductive dissolution processes on Cr^{III}_{aq} oxidation by examining the ratio of $[Mn]^T_{aq\ to}\ [Cr^{VI}]_{aq}$ resulting after different reaction conditions. It is instructive to initially consider a hypothetical reaction in which equal amounts of aqueous manganese are produced by acidic and reductive dissolution, and assuming no Cr uptake. These conditions may be described by combining Eqn. 2 (times three) and Eqn. 3 to yield Eqn. 6. Under these conditions a $[Mn]^T_{aq}$:$[Cr^{VI}]_{aq}$ ratio of 6 is expected and $3Mn^{3+}_{aq}$ are produced.

$$CrOH^{2+}_{aq} + 6\gamma\text{-MnOOH} + 9H^+ - HCrO^-_{4\,aq} + 3Mn^{3+}_{aq} + 3Mn^{2+}_{aq} + 3OH^- + 6H_2O \quad (6)$$

If we assume that in the presence of manganite each of the three Mn^{3+}_{aq} are reduced during the oxidation of $CrOH^{2+}_{aq}$ to produce $HCrO_4^-{}_{aq}$, then the $[Mn]^T_{aq}$:$[Cr^{VI}]_{aq}$ ratio would decrease to 3. In addition, given that Cr uptake does occur and the rates of acidic dissolution and reductive dissolution are generally not equal, the $[Mn]^T_{aq}$:$[Cr^{VI}]_{aq}$ ratio would be interdependent on the extent of each of these reactions (Eqn. 1 to 5). At low pH (e.g., 3) the ratio would be greatest because of the increased rate of acidic dissolution. At higher pH (e.g., 6) where there is less manganite dissolution and $CrOH^{2+}_{aq}$ oxidation competes with $Cr(OH)_3{\cdot}3H_2O$ precipitation, the ratio would likely decrease. This general behavior of the reaction stoichiometry with increasing pH is consistent with our results (Figs. 2 to 4). After ~6 h of reaction at pH 3, 4, 5 and 6, the $[Mn]^T_{aq}$:$[Cr^{VI}]_{aq}$ ratio decreased from greater than to less than 4 (4.4, 3.7, 3.1 and 2.1, respectively). Eary and Rai (1987) observed a similar trend in the $[Mn]^T_{aq}$:$[Cr^{VI}]_{aq}$ ratio, which they ascribed, as we do, to these simultaneous reactions. How-

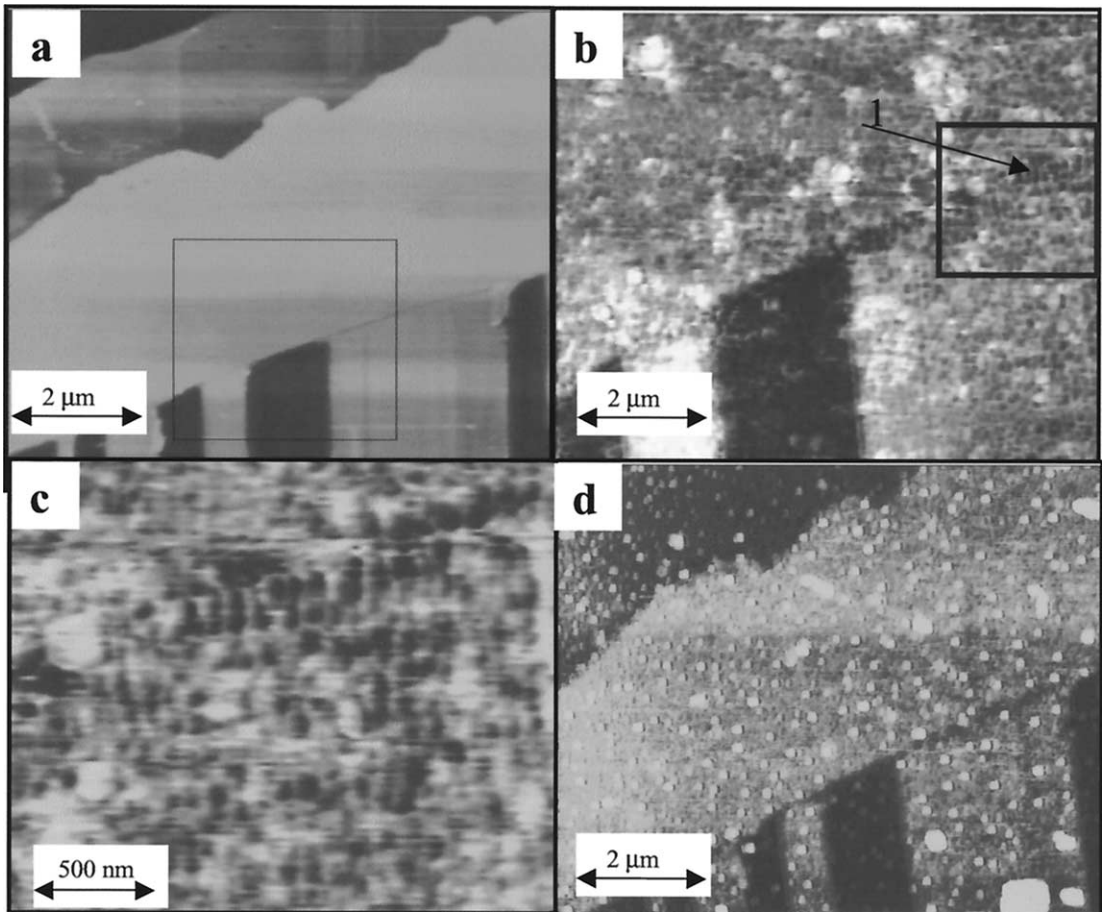

Fig. 13. Comparison of fluid-cell TMAFM images obtained in pH 4.5 HNO_3 at t = 0 (a) and after exposure to a pH 4.5, 10^{-2} M Cr^{III}_{aq} (b–d). (b) Image was obtained within 4 min of exposure. The adsorbates/microprecipitates (bright patches) are ~0.5 to 7 nm high. Note that dissolution is slightly more extensive along the step edge marked "1" in (b) and enlarged in (c). (c) Enlarged view of area outlined in (b). Dissolution pits are ~1 nm deep and are elongate along [001]. (d) AFM image collected in air after the sample has been reacted for 10 h. The surface is now extensively covered by $Cr(OH)_3{\cdot}3H_2O$ precipitates (identified by XPS), some measuring 50 nm high.

ever, other studies have found the $[Mn]^T_{aq}$:$[Cr^{VI}]_{aq}$ ratio to be in agreement with their proposed stoichiometric reactions, even at varied solution conditions (Amacher and Baker, 1982; Johnson and Xyla, 1991; Fendorf and Zasoski, 1992).

4.2. Cr Adsorption

Although not specifically addressed in this study, the driving force for Cr-adsorption on manganite is probably due to a specific (inner sphere) interaction. This is apparent from EXAFS studies on similar systems (Manceau and Charlet, 1992) and also because Cr^{3+} adsorption takes place even on positively charged surfaces. Considering manganite has a positive surface charge for pH < 5.2 (i.e., the PZC) it would be expected that the anionic chromate species ($HCrO_4^-$) formed during the oxidation of $CrOH^{2+}$ would be electrostatically bonded to the surface. However, Cr^{6+} was not detected (by XPS) on the manganite surface; only Cr^{3+} was detected. The absence of bound Cr^{6+} may be explained first by the much increased solubility of chromate (i.e., Cr^{6+} species) relative to $CrOH^{2+}_{aq}$ as a result of oxidative dissolution, which therefore disposes chromate to be predominately in an aqueous state, and second by an absence of appropriate absorption sites (e.g., tunnel, interlayer) in manganite. Interestingly, birnessite (PZC ~1.9) surfaces were shown by Banerjee and Nesbitt (1999) to sorb both cationic $CrOH^{2+}$ and anionic $HCrO_4^-$ species at a pH of ~4.6 where the surface would have a negative charge. These observations suggest that electrostatic forces acting between aqueous chromium and Mn-oxide may not have a strong influence on Cr uptake.

On the basis of the Cr^{III}_{aq} speciation study of Rai et al. (1987), $Cr(OH)^{2+}_{aq}$ is the dominant species under the reaction conditions (Fig. 1). It is proposed that this species binds preferentially at the surface hydroxyl sites of manganite. This is likely because hydroxyl sites would exhibit a slightly more basic localized environment that would be more likely to favor Cr-hydroxy hydrate nucleation.

4.3. Heterogeneity of Reaction

In situ AFM and ex situ FESEM observations show that Cr_{aq}-manganite interactions are highly heterogeneous, with

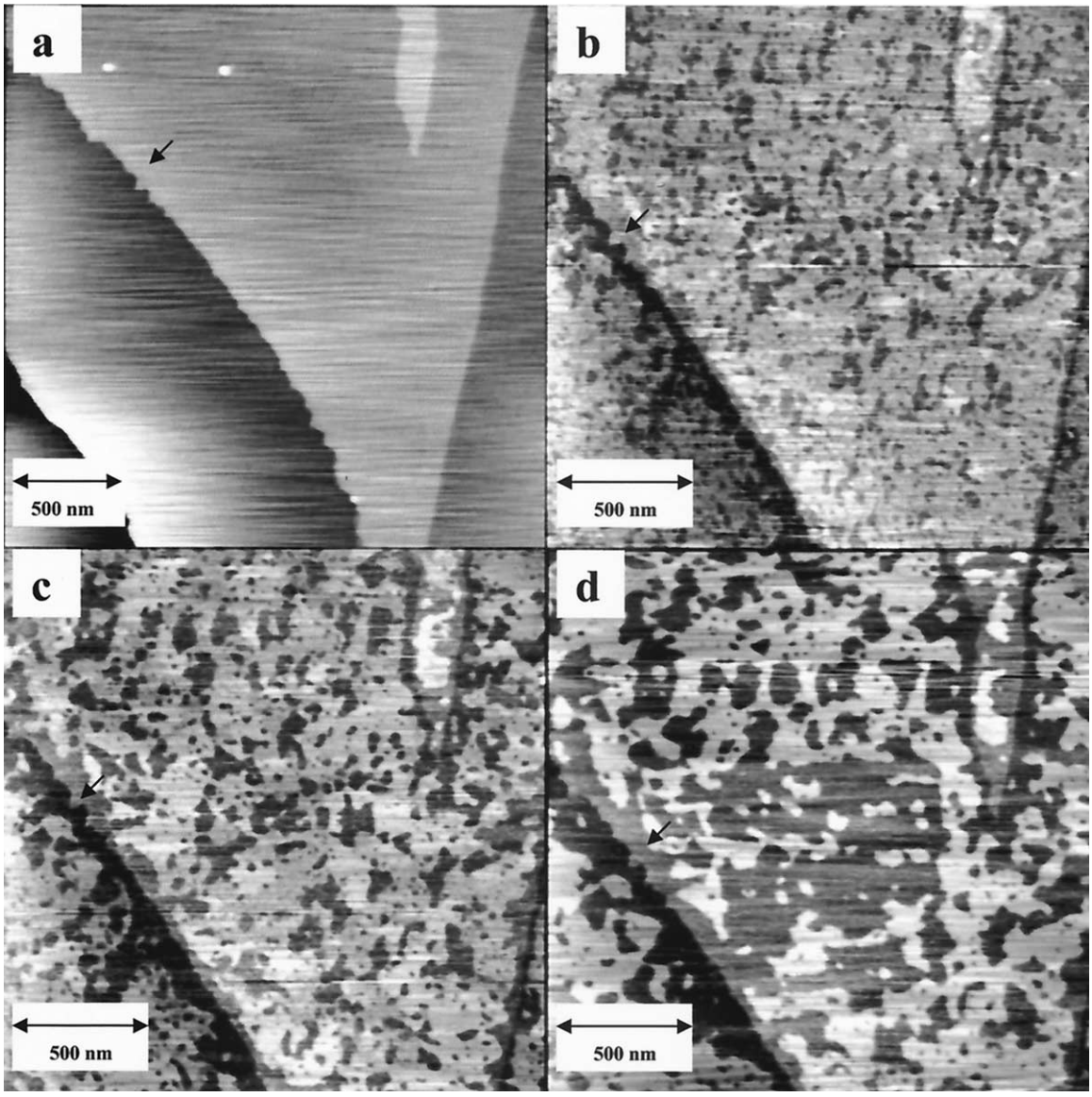

Fig. 14. Sequence of TMAFM images obtained before and during the acidic dissolution of manganite. (a) In-air image of a fresh manganite surface (t = 0). (b) Same area as (a), except slightly magnified, obtained in solution, after 13 min of exposure to pH 3.5 HNO_3. Although pitting of the terraces is widespread, dissolution is more rapid along step edges, as evidenced by the laterally continuous pits extending parallel to these edges. (c) Continued dissolution (t = 25 min) has occurred primarily at step edges, causing the pits seen in (b) to become broader. A tip radius of ~5 nm can be estimated from the diameter of the smallest resolvable pit (~10 nm). At least five terrace levels are identified, each of which is vertically offset by 0.5 ± 0.1 nm. (d) After 60 min of exposure (image area shifted up ~200 nm), many of the pits seen in (c) have now coalesced. The arrows shown in each image mark a feature that persists throughout the reaction with little to no dissolution. Tip-enhanced dissolution caused during a previous 1.0-mm scan is apparent in the central portion of the image.

some manganite surfaces showing localized microprecipitation and/or dissolution, and adjacent areas exhibiting little or no evidence for any reaction. The extent of this heterogeneity varies from sample to sample and may be dependent on a variety of physical and chemical attributes (e.g., defects, trace element dopants, twinning, micropores) and their affects on the electronic properties of the surface (e.g., band gap, electron mobility, work function). Two lines of direct evidence observed in this study demonstrate that the conductivity of manganite varies across its surface: first, differential charging as revealed in voltage contrast SEM imaging, and second, unreliable engagement of an scanning tunneling microscope tip with manganite, depending on the exact area of tip approach. The numerous factors that contribute to heterogeneous semiconductor properties preclude drawing any unambiguous conclusions. However, if electron mobility is locally inhibited on the manganite surface, then adsorbed Cr^{3+} is unlikely to be oxidized. This situation may allow for the formation of single or multinuclear $Cr(OH)_3 \cdot 3H_2O$ complexes that may accumulate to form surface clusters (Bleam and McBride, 1985) or surface

precipitates (Fendorf et al., 1992; Fendorf and Zasoski, 1992). Results of our FESEM and in situ AFM experiments are consistent with the hypothesis that variations in surface conductivity may promote $Cr(OH)_3 \cdot 3H_2O$ surface precipitation.

It has been observed in many experiments that $Cr(OH)_3 \cdot 3H_2O$ precipitates are often not spatially associated with sites of dissolution. It is logical that precipitation would tend not to occur near sites of manganite dissolution because dissolution would require either Mn-reduction (for reductive dissolution) or Mn-protonation (for acidic dissolution) that would interfere with $Cr(OH)_3 \cdot 3H_2O$ precipitation.

For areas of the manganite surface where electron transfer is not inhibited, we expect that electrons originating from an inner spherically bound Cr^{3+} are conducted into the manganite. This transfer of electrons results in the formation and subsequent desorption of chromate and either manganite dissolution localized at the Cr-adsorption site, or dissolution occurring at some other surface site, perhaps even spatially distant from the Cr-adsorption site. Heterogeneous Cr uptake and manganite dissolution behaviors such as we have observed are not uncommon in some metallic corrosion processes (Scully, 1990; Stumm and Morgan, 1996, and references therein). In addition, there is a growing base of STM and AFM observations and supporting quantum mechanical calculations that show that redox reactions occurring on semiconducting mineral surfaces are often spatially heterogeneous (Junta and Hochella, 1994; Becker et al., 1997; Rosso and Hochella, 1997; Rosso et al., 1999 a,b). These findings have recently been formulated into what has been termed the proximity effect (Becker et al., 2001). The idea is that as a result of the delocalized nature of electrons in semiconducting materials, a reducing or oxidizing chemical species at a surface site not only influences the electronic structure of neighboring sites, but also may influence other sites some distance away through electron transfer processes. In the case of Cr^{3+} adsorption and oxidation on manganite surfaces, this tells us that electron transfer from Cr to Mn need not necessarily involve only next nearest neighbor metal atoms. In fact, electrons donated by sorbed Cr atoms may travel in the conduction band of the manganite to a Mn site, for example, at a surface step or kink site some distance away where the reduced Mn will desorb, eventually forming a dissolution pit at that location after multiple transfers.

4.4. Environmental Implications

Our experiments show that in undersaturated $Cr(OH)_3 \cdot 3H_2O$ solutions, the reaction between manganite and Cr^{III}_{aq} efficiently oxidizes Cr^{III}_{aq} to Cr^{VI}_{aq} (especially at low pH or low to negative SI) with a simultaneous decrease in the $[Cr]^{T}_{aq}$ as a result of Cr adsorption and surface-catalyzed precipitation of $Cr(OH)_3 \cdot 3H_2O$. The chromate production results in a significant increase in solution toxicity (Nriagu and Nieboer, 1988). In the natural environment, this threat of increased toxicity is often reduced by competing or parallel processes such as the following: (1) passivation of the Mn-oxide surface by metal sorbates and precipitates (Fendorf et al., 1993; Pratt et al., 1997); (2) complexation of Mn^{III}_{aq} with organic and inorganic ligands (Johnson and Xyla, 1991; Nico and Zasoski, 2000); (3) bulk precipitation of $Cr(OH)_3 \cdot 3H_2O$; and (4) the presence of reductants (e.g., natural organic matter, Fe^0, Fe^{2+}-containing phases) (Powell et al., 1995; Blowes et al., 1997; Peterson et al., 1997; Jardine et al., 1999). The relative importance of each of these competing processes is dictated by the presiding aqueous and mineralogical conditions. Through much laboratory and field experimentation, it has been shown that the extent and rate of Cr^{III}_{aq} oxidation is greatest in environments of low pH and high Mn-oxide content. Given this knowledge, appropriate geochemical conditions for safe chromium disposal include slightly basic to neutral pH; the absence of Mn-oxides; and the presence of a strong reductant (e.g., Fe^0). Satisfying more than one of these conditions provides added security that chromium remains in the relatively immobile and nontoxic Cr^{III}_{aq} or $Cr(OH)_3 \cdot 3H_2O_{(s)}$ state.

Acknowledgments—This work was supported by grants from the NSF (EAR 96-9628023, 99-9902996, and 9975678) and The American Federation of Mineralogists. We thank Don Rimstidt and Matt Eick of Virginia Tech for insightful comments.

Associate editor: D. L. Sparks

REFERENCES

Amacher M. C. and Baker D. A. (1982) Redox Reactions Involving Chromium, Plutonium and Manganese in Soils. Institute for Research on Land and Water Resources, Pennsylvania State University.

Banerjee D. and Nesbitt H. W. (1999) Oxidation of aqueous Cr(III) at birnessite surfaces: Constraints on reaction mechanism. *Geochim. Cosmochim. Acta* **63,** 1671–1687.

Becker U., Hochella M. F. Jr., and Vaughan D. J. (1997) The adsorption of gold to galena surfaces: Calculation of adsorption/reduction energies, reaction mechanisms, XPS spectra, and STM images. *Geochim. Cosmochim. Acta* **61,** 3565–3585.

Becker U., Rosso K. M., and Hochella M. F. Jr. (2001) The proximity effect on semiconducting mineral surface: A new aspect of mineral surface reactivity and surface complexation theory? *Geochim. Cosmochim. Acta* **65,** 2641–2649.

Bleam W. F. and McBride M. B. (1985) Cluster formation versus isolated-site adsorption: A study of Mn(II) and Mg(II) adsorption on boehmite and goethite. *J. Colloid Interf. Sci.* **103,** 124–132.

Blowes D. W., Ptacek C. J., and Jambor J. L. (1997) In-situ remediation of Cr(VI)-contaminated groundwater using permeable reactive walls: Laboratory studies. *Environ. Sci. Technol.* **31,** 3348–3357.

Buerge I. J. and Hug S. J. (1999) Influence of mineral surfaces on chromium(VI) reduction by iron(II). *Environ. Sci. Technol.* **33,** 4285–4291.

Burns R. G. and Burns V. M. (1979) Manganese oxides. *Rev. Mineral.* **6,** 1–46.

Chao T. T. and Anderson B. J. (1974) The scavenging of silver by manganese and iron oxides in stream sediments collected from two drainage areas of Colorado. *Chem. Geol.* **14,** 159–166.

Chung J.-B. (1998) Chromium speciation in Cr(III) oxidation by Mn-oxides: Relation to the oxidation mechanism. *Han'guk Nonghwa Hakhoechi* **41,** 89–94.

Chung J.-B., Zasoski R. J., and Lim S.-U. (1994) Kinetics of chromium(III) oxidation by various manganese oxides. *Han'guk Nonghwa Hakhoechi* **37,** 414–20.

Dillard J. G. Koppelman M. H. Crowther D. L. Schenck C. V. Murray J. W. and Balistrieri L. (1981) X-ray photoelectron spectroscopic (XPS) studies on the chemical nature of metal ions adsorbed on clays and minerals. In *Adsorption Aqueous Solutions,* pp. 227–240. Virginia Department of Water Resources.

Eary L. E. and Rai D. (1987) Kinetics of chromium (III) oxidation to chromium (VI) by reaction with manganese oxide. *Environ. Sci. Technol.* **26,** 79–85.

Evans S. and Raftery E. (1982) Determination of the oxidation state of manganese in lepidolite by x-ray photoelectron spectroscopy. *Clay Mineral.* **17,** 477–81.

Fendorf S. E. and Zasoski R. J. (1992) Chromium (III) oxidation by δ-MnO_2: Characterization. *Environ. Sci. Technol.* **21,** 1187–1193.

Fendorf S. E., Fendorf M., Sparks D. L., and Gronsky R. (1992) Inhibitory mechanisms of chromium(III) oxidation by δ-manganese dioxide. *J. Colloid Interf. Sci.* **153,** 37–54.

Fendorf S. E., Zasoski R. J., and Burau R. G. (1993) Competing metal ion influences on chromium (III) oxidation by birnessite. *Soil Sci. Soc. Am. J.* **57,** 1508–1515.

Goldstein J. I., Newbury D. E., Echlin P., Joy D., Romig A. D. J., Lyman C. E., Fiori C., and Lifshin E. (1992) *Scanning Electron Microscopy and X-ray Microanalysis*. Plenum Press.

Gray M. J. and Malati M. A. (1979) Adsorption from aqueous solution by δ-manganese oxide: II Adsorption of some heavy metal cations. *J. Chem. Technol. Biotechnol.* **29,** 135–144.

Gupta R. P. and Sen S. K. (1974) Calculations of multiplet structure of core p-vacancy levels. *Phys. Rev. B* **10,** 71–79.

Gupta R. P. and Sen S. K. (1975) Calculation of multiplet structure of p-vacancy levels II. *Phys. Rev. B* **12,** 15–19.

Halada G. P. and Clayton C. R. (1991) Photoreduction of hexavalent chromium during X-ray photoelectron spectroscopy analysis of electrochemical and thermal films. *J. Electrochem. Soc.* **138,** 2921–2927.

Hem J. D. (1981) Rates of manganese oxidation in aqueous systems. *Geochim. Cosmochim. Acta* **45,** 1369–1374.

Hem J. D., Roberson C. E., and Fournier R. B. (1982) Stability of β-MnOOH and manganese oxide deposition from springwater. *Water Resources Res.* **18,** 563–570.

Hem J. D., Lind C. J., and Roberson C. E. (1989) Coprecipitation and redox reactions of manganese oxides with copper and nickel. *Geochim. Cosmochim. Acta* **53,** 2811–2822.

Ikemoto I., Ishii K., Kinoshita S., Kuroda H., Alario-Franco M. A., and Thomas J. M. (1976) X-ray photoelectron spectroscopic studies of chromium dioxide and some related chromium compounds. *In J. Solid State Chem.* **17,** 425–430.

Ilton E. S., Veblen D. R., Moses C. O., and Raeburn S. P. (1997) The catalytic effect of sodium and lithium ions on coupled sorption-reduction of chromate at the biotite edge–fluid interface. *Geochim. Cosmochim. Acta* **61,** 3543–3563.

Jardine P. M., Fendorf S. E., Mayes M. A., Larsen I. L., Brooks S. C., and Bailey W. B. (1999) Fate and transport of hexavalent chromium in undisturbed heterogeneous soil. *Environ. Sci. Technol.* **33,** 2939–2944.

Johnson C. A. and Xyla A. G. (1991) The oxidation of chromium(III) to chromium(VI) on the surface of manganite (γ-MnOOH). *Geochim. Cosmochim. Acta* **55,** 2861–2866.

Johnsson P. A., Eggleston C. M., and Hochella M. F. Jr. (1991) Imaging the molecular-scale structure and microtopography of hematite with the atomic force microscope. *Am. Mineral.* **76,** 1442–1445.

Junta J. L. and Hochella M. F. Jr. (1994) Manganese(II) oxidation at mineral surfaces: A microscopic and spectroscopic study. *Geochim. Cosmochim. Acta* **58,** 4985–4999.

Kavanaugh M. C. (1994) *Alternative for Groundwater Cleanup*. National Academy Press.

Lind C. J. (1988) Hausmannite (Mn_3O_4) conversion to manganite (γ-MnOOH) in dilute oxalate solution. *Environ. Sci. Technol.* **22,** 62–70.

Malati M. A. and Rophael M. W. (1999) Radiochemical and physicochemical characterization of manganese oxides. *Surf. Sci.,* **433,** 740–744.

Manceau A. and Charlet L. (1990) In-Situ X-ray absorption study of the mechanism of Cr(III) oxidation at the Mn oxide/water interface, Geochemistry of the Earth's Surface and of Mineral Formation, 2nd International Symposium, Aix en Provence, France, 275–278.

Manceau A. and Charlet L. (1992) X-ray absorption spectroscopy study of the sorption of Cr(III) at the oxide–water interface I: Molecular mechanisms of Cr(III) oxidation on Mn oxides. *J. Colloid Interf. Sci.* **148,** 425–442.

McKenzie R. M. (1967) The sorption of cobalt by manganese minerals in soils. *Aust. J. Soil Res.* **5,** 235–246.

McKenzie R. M. (1980) The adsorption of lead and other heavy metals on oxides of manganese and iron. *Aust. J. Soil Res.* **18,** 61–73.

Means J. L., Crerar D. A., Borcsik M. P., and Duguid J. O. (1978) Adsorption of Co and selected actinides by Mn and Fe oxides in soils and sediments. *Geochim. Cosmochim. Acta* **42,** 1763–1773.

Murray D. J., Healy T. W., and Fuerstenau D. W. (1968) The adsorption of aqueous metal on colloidal hydrous manganese oxide. In *Adsorption from Aqueous Solution*, Vol. 79 (eds. W. J. Weber Jr and E. Matijevic), pp. 74–87. American Chemical Society.

Murray J. W. and Dillard J. G. (1979) The oxidation of cobalt(II) adsorbed on manganese dioxide. *Geochim. Cosmochim. Acta* **43,** 781–787.

Murray J. W., Dillard J. G., Giovanoli R., Moers H., and Stumm W. (1985) Oxidation of Mn(II): Initial mineralogy, oxidation state and ageing. *Geochim. Cosmochim. Acta* **49,** 463–470.

Nesbitt H. W., Banerjee D. (1988) Interpretation of XPS Mn (2p) spectra of Mn oxyhydroxides and constraints on the mechanism of MnO_2 precipitation, *Am. Mineralogist* **83,** (3-4), 305–315.

Nico P. S. and Zasoski R. J. (2000) Importance of Mn(III) availability on the rate of Cr(III) oxidation on δ-MnO_2. *Environ. Sci. Technol.* **34,** 3363–3367.

Nriagu J. O. and Nieboer E. (1988) Advances in Environmental Science and Technology, Vol. 20: Chromium in the Natural and Human Environments, American Chemical Society.

Peterson M. L., Brown G. E. Jr., Parks G. A., and Stein C. L. (1997) Differential redox and sorption of Cr(III/VI) on natural silicate and oxide minerals: EXAFS and XANES results. *Geochim. Cosmochim. Acta* **61,** 3399–3412.

Powell R. M., Puls R. W., Hightower S. K., and Sabatini D. A. (1995) Coupled iron corrosion and chromate reduction: Mechanisms for subsurface remediation. *Environ. Sci. Technol.* **29,** 1913–1922.

Pratt A. R. and McIntyre N. S. (1996) Comment on curve fitting of Cr 2p photoelectron spectra of Cr_2O_3 and CrF_3. *Surf. Interface Anal.* **24,** 529–530.

Pratt A. R., Blowes D. W., and Ptacek C. J. (1997) Products of Chromate Reduction on Proposed Subsurface Remediation Material. *Environ. Sci. Technol.* **31,** 2492–2498.

Rai D., Sass B. M., and Moore D. A. (1987) Chromium(III) hydrolysis constants and solubility of chromium(III) hydroxide. *Inorg. Chem.* **26,** 345–349.

Rophael M. W. and Boulis S. N. (1982) Kinetics of the oxidation of chromium(III) ions by trimanganese tetroxide and by manganese(III) oxide. *Surf. Technol.* **16,** 243–248.

Rosso K. M., Becker U., and Hochella M. F. Jr. (1999a) Atomically resolved electronic structure of pyrite{100} surfaces: An experimental and theoretical investigation with implications for reactivity. *Am. Mineral.* **84,** 1535–1548.

Rosso K. M., Becker U., and Hochella M. F. Jr. (1999b) The interaction of pyrite{100} surfaces with O_2 and H_2O: Fundamental oxidation mechanisms. *Am. Mineral.* **84,** 1549–1561.

Schroeder D. C. and Lee G. F. (1975) Potential transformations of chromium in natural waters. *Water Air Soil Pollut.* **4,** 355–365.

Scully J. C. (1990) *The Fundamentals of Corrosion*. p. 226. Pergamon Press.

Silvester E., Charlet L., and Manceau A. (1995) Mechanism of chromium(III) oxidation by Na-buserite.. *J. Phys. Chem* **99,** 16662.

Stumm W. and Morgan J. J. (1996) Aquatic Chemistry: Chemical Equilibria and Rates in Natural Waters. p. 1022. Wiley.

Van Der Weijden C. D. and Reith M. (1982) Chromium(III)–chromium(VI) interconversions in seawater. *Mar. Chem* **11,** 565–572.